Hindawi
Advances in Civil Engineering
Volume 2021, Article ID 8141015, 8 pages
https://doi.org/10.1155/2021/8141015

Research Article

An Impact-Echo Experimental Approach for Detecting Concrete Structural Faults

Ya-xun Yang,[1,2] **Wen-hao Chai**,[1] **De-chuang Liu**,[1] **Wei-de Zhang**,[1] **Jia-cheng Lu**,[1] **and Zhi-kui Yang**[3]

[1]*School of Highway, Chang'an University, Xi'an, Shaanxi 710064, China*
[2]*The Engineering Design Academy of Chang'an University Company Limited, Xi'an, Shaanxi 710064, China*
[3]*School of Civil Engineering, Shaanxi Vocational and Technical College, Xi'an, Shaanxi 710100, China*

Correspondence should be addressed to Ya-xun Yang; yyx@chd.edu.cn

Received 7 November 2021; Accepted 3 December 2021; Published 20 December 2021

Academic Editor: Lingkun Chen

For the current problem of detection of grouting defects in posttensioned prestressed concrete members, the paper takes a single-layer arrangement of prestressed pipes as the object of study. The influence law of the main factors such as pipe material, defect size, defect critical surface location, and prestressing reinforcement location on the results of the impact-echo method for detecting concrete grouting defects was studied. Firstly, the ABAQUS finite element software was used to simulate these factors to obtain the influence law on the detection results, and a modal test was conducted to verify them. The results show that the impact-echo method can effectively test the location of defects and the degree of burial depth, and the pipe material influences the test results, and the impact of corrugated metal pipe is smaller and more accurate than the PVC pipe. In addition, the greater the plate thickness frequency drift rate, the larger the transverse size of the defect, so the plate thickness frequency drift rate and the measured defect depth are combined to quantitatively determine the depth of the defect.

1. Introduction

With the extensive use of posttensioned prestressed concrete bridges, the compactness of posttensioned prestressing duct grouting has become a major problem affecting the performance of bridges. Poor grouting results in the corrosion of prestressing steel bars, and consequently, the collapse of bridge structures has occurred frequently in the past decades. There have been publicly watched bridge collapses in recent years, including the Ynys-y-gwas in South Wales [1], Malle Bridge in Belgium [2], and Tian Zhuang Tai Bridge across the Daliao River on U.S. Route 305 [3]. The investigation shows that the lack of compactness of grouting causes the collapse. To solve this problem, the commonly used methods of grouting compactness detection such as rebound method, ultrasonic method, ground penetrating radar (GPR), acoustic scattering tracking method, endoscopy method, thermal infrared imaging method, and impact-echo (IE) method are used [4–7].

The IE method is a standard nondestructive testing method for detecting the surface and subsurface defects in concrete structures. The technique is widely used in practical engineering because of its convenient and straightforward testing process. It is also known as the most promising inspection method. The impact-echo method was first proposed by Cornell University in the 1980s and used the method to detect defects in prestressed pipes [8].

Hill et al. carried out an experimental study on the quality of prestressed pipe grouting using the impact-echo method of detection. They found that the technique could effectively identify signals of grout defects in square beam pipes [9]. Liu et al. [10] and Kang et al. [11] found that defects in reinforced concrete structures could be accurately detected using the shock-echo method through an indoor experimental study. Jiang et al. [12] used the IE method to detect the concrete emptying problem, and the results showed that the technique was feasible. The impact-echo method analyzes IE data and requires user expertise to define the analysis parameters, hindering comprehensive field implementation.

The feasibility of using deep learning models (DLMs) to detect concrete structural defects has been recently investigated [13]. In this paper, based on this research, the factors affecting the detection results of the impact-echo method are numerically simulated using ABAQUS and validated by indoor tests.

2. Principle of IE Method

The impact-echo method is a method to detect defects using low-frequency stress waves generated by transient shock. In practical engineering, a small steel ball is usually used to tap the surface of the concrete. At this time, a stress wave will be generated on the surface of the concrete. The stress wave (mainly P wave) propagates to the structure, and the reflection phenomenon will occur at different media interfaces. The back-and-forth reflection between other interfaces produces transient resonance. The stress wave formed by transient resonance changes the surface displacement of the concrete structure. Then, the displacement signal is received by the sensor placed near the impact point. The displacement signal received by the sensor is transformed into a frequency domain signal after fast Fourier transform (FFT). Finally, the time-domain signal is transformed into a frequency-domain signal according to the received signal. Frequency-domain signals are used to determine the size and density of defects in the structure. The schematic diagram of the detection principle is shown in Figure 1.

According to the principle of the impact-echo method [14–17], the equations for calculating thickness and frequency are different for different impedance materials when analyzing frequency signals. For compact flawless concrete slabs, the thickness frequency (F_T) can be determined by equation (1), and for reinforced concrete, the reflection frequency (F_s) can be determined by equation (2) as follows:

$$F_T = \alpha_s \frac{V_p}{2T}, \tag{1}$$

$$F_s = \alpha_s \frac{V_P}{4d}, \tag{2}$$

where α_s represents the shape coefficient of the slab; for concrete slab, it is generally 0.96; V_p represents the wave velocity of stress wave in concrete when propagating; T represents the thickness of the slab; d represents the depth of the channel.

Based on equation (2), the impact-echo signals collected from the nonprestressing pipe section, grouting channel, and nongrouting channel specimens in the concrete slab will show different characteristics when the grouting compactness of the channel is tested (Figure 2).

3. Finite Element Simulation

3.1. Introduction to Simulation. The impact response under different working conditions is simulated and analyzed by using the finite element software, ABAQUS display solver. The impact-echo method studied the specific influence of various typical factors on the accurate positioning and quantitative detection of grouting defects in prestressed concrete structures. In the study, the impact load generated by steel ball impact is simplified to a semiperiodic simple harmonic force directly. It is inspected at a distance of 5 cm near the impact point. Acceleration/displacement of the measured surface is used to obtain the response signal of the stress wave propagating in concrete. Finally, the received time-domain signal is transformed into a frequency-domain signal through fast Fourier transform (FTT), and the spectrum chart is drawn.

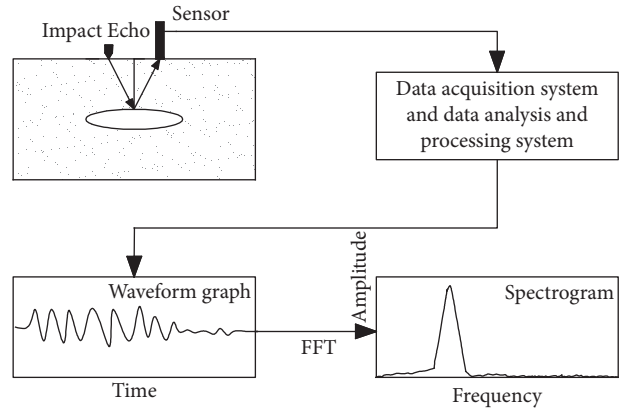

Figure 1: Schematic diagram of the shock-echo method.

3.2. Simulation Parameters. For the ABAQUS simulation, the material parameters are selected, as shown in Table 1.

In the experimental study, C40 concrete is selected; the meshing accuracy is 10 mm; the impact steel ball with a diameter of 6 mm is used; the impact load is regarded as a half-period sinusoidal load, in which the maximum concentrated force is 30 N, and the impact duration is 30us. The concrete relationship is shown in the following equation:

$$F = F_{\max} \sin\left(\frac{\pi t}{t_c}\right). \tag{3}$$

In the above equation, F is the action force of t at a specific time, $F_{\max}$ is the maximum load of 30 N, t is the action time range of 1–30 μs, and t_c is the impact duration.

3.3. Simulated Working Conditions. To study the typical influence factors of pipeline material, defect size, defect critical plane position, and prestressing steel bundle, the following working conditions were set up as follows: (1) different grouting degrees was arranged to simulate different defect sizes; the hollow four working conditions such as compactness, 1/3 grouting, 1/2 grouting, and 2/3 grouting were set (see model 1–4 in Table 2), and the other conditions were the same. (2) Parallel and vertical working conditions of critical defect surface and test surface were arranged (see model 5–6 in Table 2), (3) To study the influence of the position of prestressing tendons and tendons on test results, two working conditions of prestressing tendons are set up at the top of the pipeline and the bottom of the pipeline, respectively (see model 7–10 in Table 2).

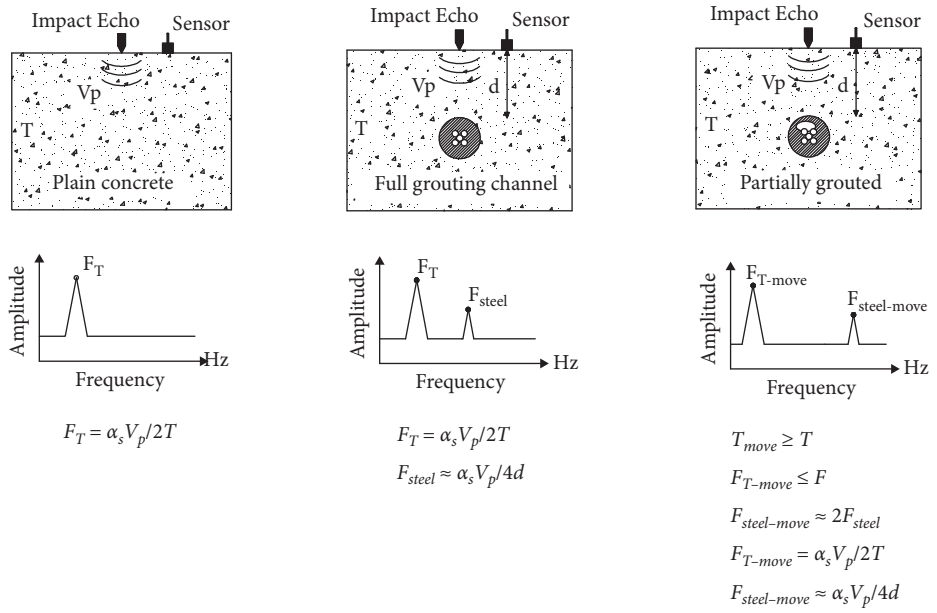

Figure 2: Response spectrum analysis diagram of different channels.

Table 1: Material parameters.

Material	Density (Kg/m^3)	Elastic modulus (Pa)	Poisson's ratio
Steel	7.8×10^3	2.1×10^{11}	0.3
Concrete	2.4×10^3	3.25×10^{10}	0.2
Mortar	1.74×10^3	8.71×10^9	0.2
PVC	1.1×10^3	4×10^9	0.2

Note. PVC, polyvinyl chloride.

Table 2: Summary of working condition model parameters.

Model number	Corrugated pipe material	Grouting compactness	Position of the critical surface of the defect (and the test surface)	Prestressed tendons and their position
1	Metal/PVC	Not grouted	Parallel	None
2	Metal/PVC	1/3Grouting	Parallel	None
3	Metal/PVC	2/3Grouting	Parallel	None
4	Metal/PVC	Compact	Parallel	None
5	Metal	1/3Grouting	Vertical	None
6	Metal	2/3Grouting	Vertical	None
7	Metal	Compact	Parallel	Exist (pipe top)
8	Metal	Compact	Parallel	Exist (pipe bottom)
9	Metal	1/2Grouting	Parallel	Exist (pipe top)
10	Metal	1/2Grouting	Parallel	Exist (pipe bottom)

Note. In Table 2, the location of the defective critical surface is parallel to the test surface that is "top and bottom plate conditions" and vertical that is "web condition."

Figure 3 is a partial model diagram. The finite element model is 1.6 m in length, 0.4 m in width, and 0.3 m in height. The pipes are arranged in the central position. The diameter of the pipes is 80 mm, the thickness of the metal wave tube wall is 2 mm, the thickness of the PVC pipe wall is 3 mm, and the diameter of the prestressed steel bar bundle is approximately simulated with a 4 cm steel bar. The working conditions are summarized in Table 2.

3.4. Simulation Results. The set working conditions are simulated numerically. The time-domain signal data of test points are collected. The time-domain signal data are converted into frequency-domain signals by fast Fourier transform with MATLAB data processing software.

The spectrum of each working condition is obtained. Some of the spectrum results are shown in Figure 4. The peak values in the spectrum of all operating conditions are

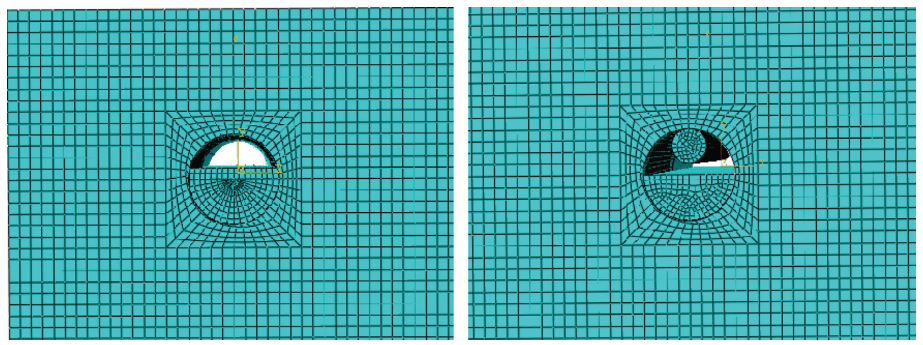

Figure 3: Schematic diagram of the finite element model.

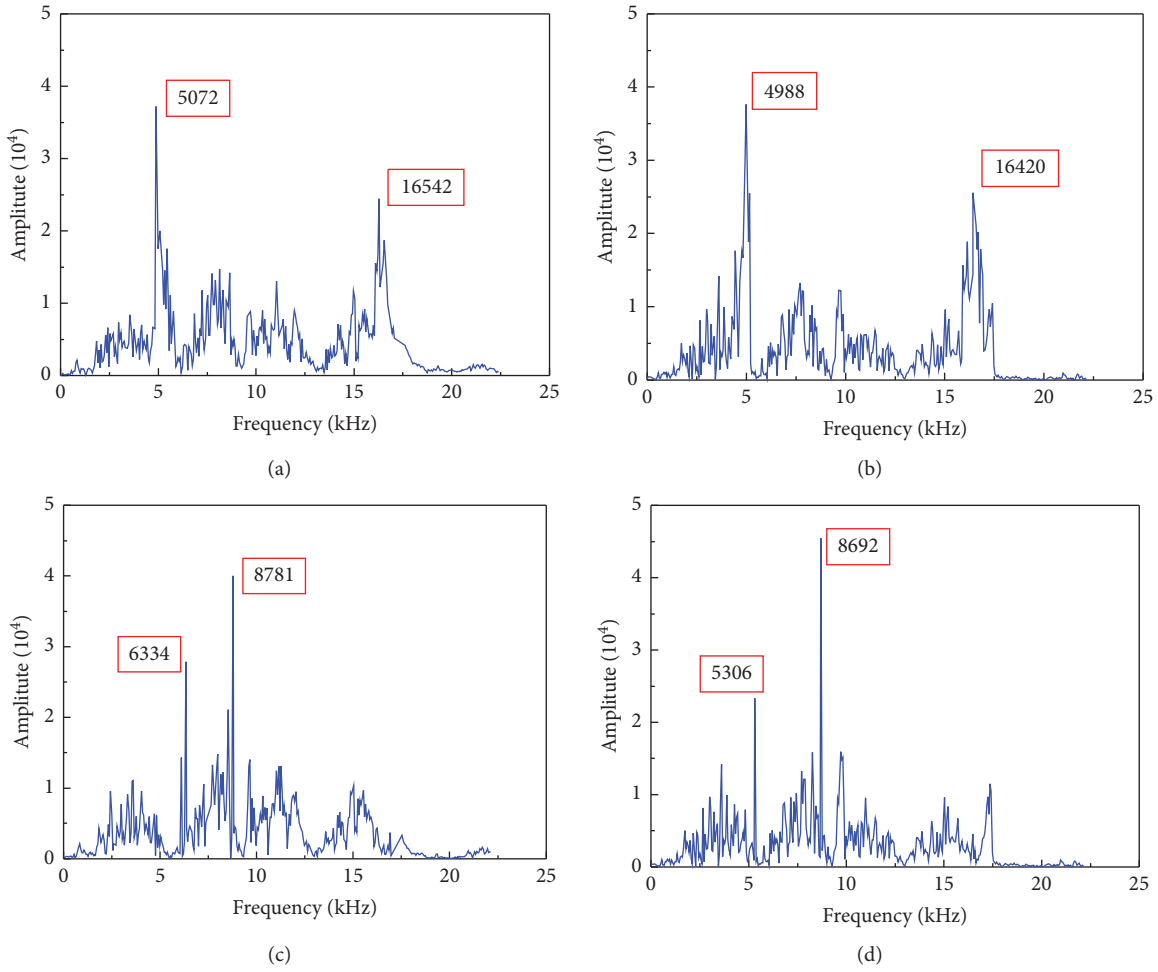

Figure 4: Parts of the spectrogram. (a) 3-spectrogram of metal bellows; (b) 4-spectrogram of metal bellows; (c) 7-spectrogram of metal bellows; (d) 9-spectrogram of metal bellows.

counted, and the corresponding thickness frequency values, defect thickness frequency values, and drift rates (Δ f and Δ F) are calculated according to equation (1) or equation. (2). The peak frequency results are shown in Table 3.

By comparing the results of 1–1~4–2 in Table 3, it can be seen that when the pipe grouting is defective, the corresponding plate thickness frequency drifts to the low frequency, and the drift rate increases gradually with the increase of the defect size; this point can be used as a basis for judging whether there are defects in the prestressed pipeline. The drift rate of metal bellows increased from 2.1% to 19.6%; the drift rate of PVC pipe increased from 2.5% to 24.7%, and the error of corresponding defect reflection frequency of metal pipe was smaller than that of PVC pipe, which shows that the material bellows have an effect on the test results. Under the same conditions, the obstruction of metal bellows

Table 3: Peak frequency.

Number	Plate thickness frequency			Defect frequency		
	f_{theory}	$f_{calculate}$	Δf (%)	F_{theory}	$F_{calculate}$	ΔF (%)
1–1	6206.3	4988.0	19.6	16296.4	16420	3.0
2–1		5072.0	18.3	16296.4	16542	2.3
3–1		5233.0	15.7	16296.4	16485	2.6
4–1		6080.0	2.1	/	/	/
1–2		4673.0	24.7	16296.4	16180	4.4
2–2		4821.0	22.3	16296.4	16277	4.1
3–2		4904.0	20.9	16296.4	16331	3.5
4–2		6053.0	2.5	/	/	/
5		5581.0	10.1	16477	16025	2.7
6		5883.0	5.2	16477	15810	4.1
7		6334.0	−2.1	/	/	/
8		6334.0	−2.1	/	/	/
9		5306.0	14.5	13299.2	12768.5	3.8
10		5306.0	14.5	16926.4	16255.0	3.9

Notes. (1) 1–1 in the table is a corrugated metal pipe; 1–2 is the PVC corrugated pipe; the rest are similar. The rest of the number corresponds to the working conditions in Table 2. (2) "/" in the table indicates that there is no such content, and the above frequency unit is kHz. (3) $\Delta f = (f_{theory} - f_{calculate})/f_{theory}$; $\Delta F = (F_{theory} - F_{calculate})/F_{theory}$; Δ F takes absolute value.

is less than that of PVC pipes, and the results are closer to the theoretical values. Therefore, metal pipes can be used as grouting channels.

By comparing the results of 1–1 ~ 4–1, 5, and 6 in Table 3, it can be seen that, under the condition of the web, the frequency drift rate of plate thickness measured under the condition of the same defect size as that of the top and the bottom plates is smaller than that of top and bottom plates. This is because when the critical surface of the defect is perpendicular to the test surface (web condition), the transverse dimension of the fault is much smaller when the transverse size of the defect is parallel (top and bottom state); when the frequency drift rate of the thickness of the plate is more significant, the transverse dimension of the defect (the depth of the defect at the top of the pipeline) is more meaningful, and vice versa, and the difficulty of detection is increased.

Through comparative analysis of the results of 7–10 in Table 3 and *c* and *d* in Figure 4, it can be found that the frequency of plate thickness shifts. When the prestressed steel bundle is located on the top of the pipe, the reflection frequency of the steel bundle can be detected, which are 8781.0 kHz and 8692.0 kHz, respectively, which are close to the theoretical value 8463.1 kHz, and the reflection frequency of the steel bundle cannot be measured when the upper hole appears. However, the measurement of the depth frequency of the defect will not be disturbed. In addition, it is found that when the steel bundle is laid at the bottom of the pipeline, the reflection frequency of the steel bundle can easily overlap with the frequency of plate thickness under the condition of dense grouting, and the peak frequency cannot be displayed.

4. Field Tests

4.1. Specimen Preparation. In order to validate the findings of the finite element modeling investigation, three C40 concrete slab specimens were fabricated outdoors. The plate was 1.6 m × 1 m × 0.3 m in size(length×width×height) (1 piece) and 0.8 m × 1 m × 0.3 m in size (length × width × height) (2 pieces). The former was used to validate the effect of pipe material and defect size on the influence law. The latter was utilized to validate the influence law between the position of a trapped critical surface and a prestressing steel beam. Each specimen has 4 orifices. The pipe diameter is set to φ80 mm; the center of the pipe is 110 mm from the surface of the sample, and in the third plate, another φ8 standard reinforcement is arranged with a spacing of 5 cm. 3φ16 standard reinforcement bundles are selected instead of the prestressing steel bundles, and the dimensional diagram of specimen 1 is shown in Figure 5(a), and the field specimen is shown in Figure 5(b). The longitudinal arrangement of specimens 2 and 3 is the same as that of specimen 1. The transverse dimensions of the grouting are as described in Table 2.

4.2. Testing Process. The concrete slab surface corresponding to the longitudinal axis of each pipeline is selected as the test line of pipeline grouting with a diameter of 6 mm. The test spacing is 10 cm in the longitudinal direction without considering the edge point and the midpoint of the specimen. There are 14 test points in specimen 1, 7 test points in specimens 2 and 3, and the distance between the test point and the impact point should be less than 0.4 h (h is the distance between the top of the bellows and the test surface). 3 cm was selected in this experiment. Firstly, the wave velocity of each specimen is calibrated by SPC-MATS, and each sample is averaged by selecting several measuring points.

4.3. Test Results. The results of wave velocity calibration are as follows: specimen 1 is 3956.5 m/s, specimen 2 is 3988.3 m/s, and specimen 3 is 4000.2 m/s. The frequency of each measuring point is measured, and the corresponding thickness frequency drift rate and defect depth drift rate are calculated. The results

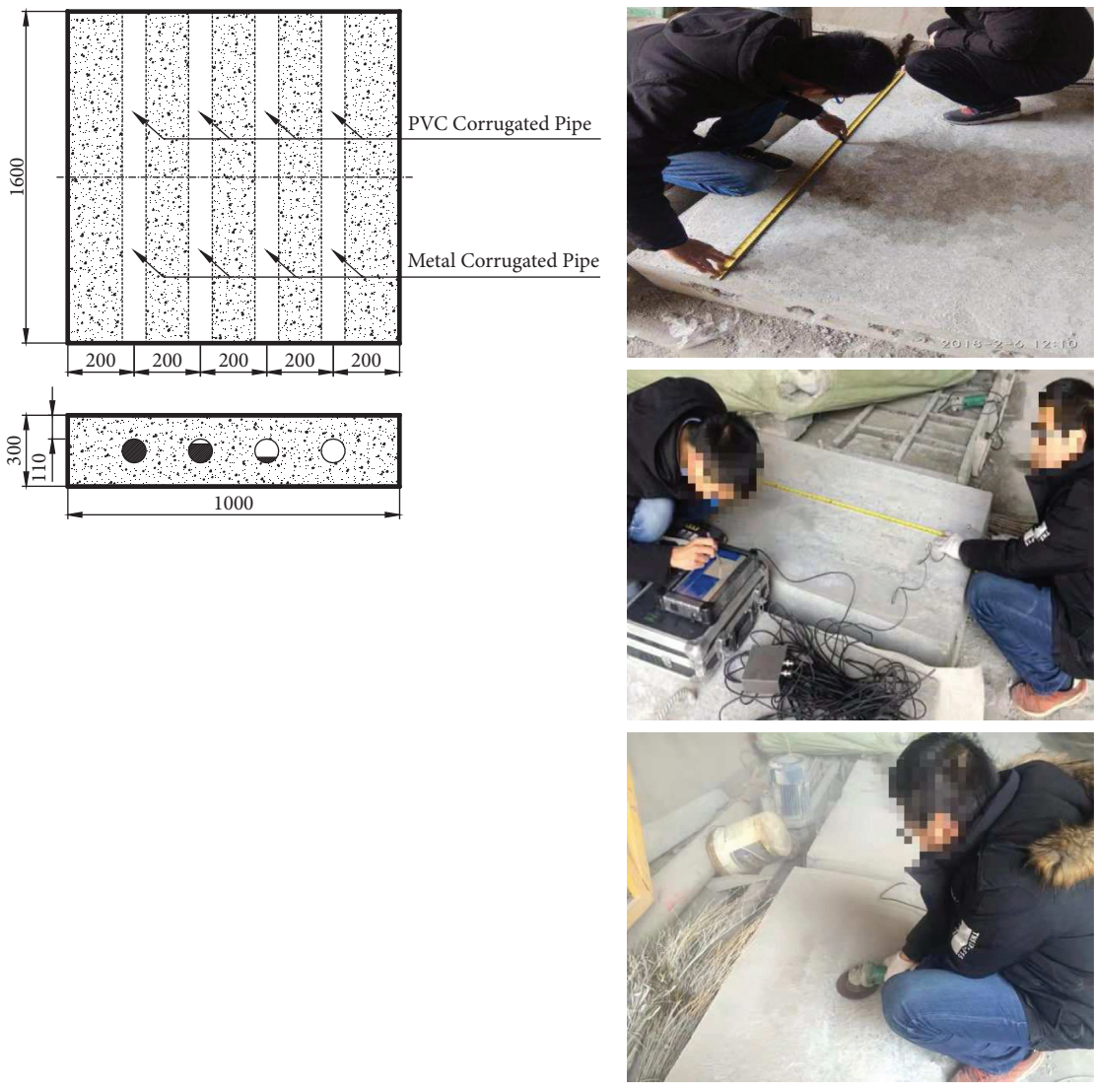

Figure 5: Schematic diagram of specimen 1. (a) Specimen size drawing. (b) On-site test piece diagram.

of points 3, 4, and 9, 10 in the No. 1 board are compared and analyzed. The results are shown in Figure 6. From Figure 6(a) and calculation, it can be seen that with the increase of defect size, the corresponding plate thickness frequency decreases gradually, and the drift rate increases slowly. In metal pipes, the drift rate of measuring point 3 is from 4.4% to 20.8%, and the drift rate of measuring point 4 is from 3.9% to 21.2%; in PVC pipes, the drift rate of measuring point 9 is from 7.5% to 27.6%, and the drift rate of measuring point 10 is from 6.5% to 27.3%; but for the defect degree error, the drift rate of measuring point 3 is calculated. The nominal defect depth is shown in Table 4. The error rate of metal bellows is between 4% and 5.5%, while PVC tubes are between 6% and 8.1%. It shows that the test result of the metal tube is more accurate.

For the metal pipelines under the vertical working conditions of No. 2 and No. 3 in the No. 2 plate, relevant data of 3 and 4 measuring points are taken. The results are shown in Table 4.

It can be seen from Table 4 that under the same defect size conditions as the top and bottom plates, the measured frequency drift rate of plate thickness is less than that under the top and bottom conditions. The error of defect depth is more significant than that of roof and floor, and there are no data at some detection points, which shows that under the same conditions, it is more difficult to detect the defect when the critical surface of the fault is perpendicular to the test surface (web condition) than when the transverse dimension of the defect is parallel (top and bottom conditions).

The plate thickness frequency and defect frequency of the measured points are counted as shown in Figure 7.

From Figure 7 and calculation, it can be found that the drift rate of plate thickness frequency is low. The drift rate of plate thickness in working conditions 7 and 8 is between 4% and 6.3%, the drift rate of plate thickness in working conditions 9 and 10 is between 15% and 18%, and the frequency of defect depth can be detected in working conditions 9 and

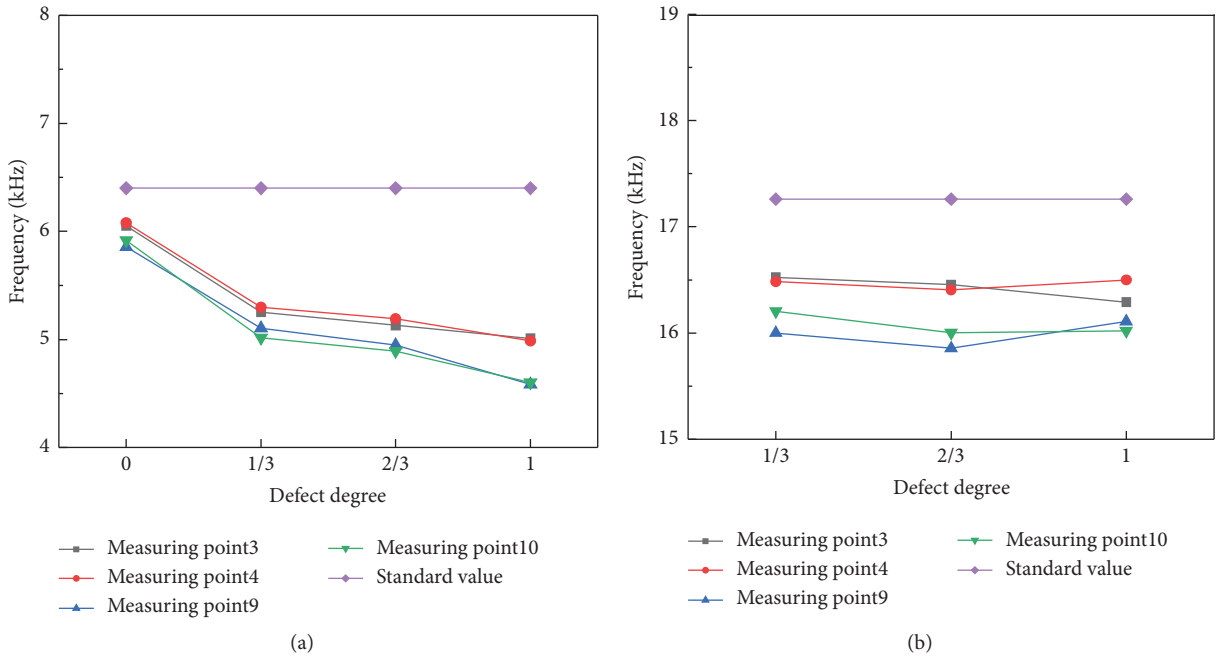

Figure 6: Frequency diagram of measuring points on the plate 1# (a) Plate thickness frequency chart (b) Defect frequency chart.

Table 4: Measurement point results of plate No. 2.

Measuring point	Working condition	f_{test}	f_{theory}	Δf (%)	F_{test}	F_{theory}	ΔF (%)
3	1/3	5409	6381	15.2	16280	17403	6.5
	2/3	5882		7.8	18943		8.8
4	1/3	5304		16.8	15986		8.1
	2/3	5943		6.9	15874		8.7

Notes. The above frequency unit is kHz. f_{test}—the test value of plate thickness frequency. f_{theory}—the theoretical value of plate thickness frequency. F_{test}—the test value of defect frequency. F_{theory}—the theoretical value of defect frequency.

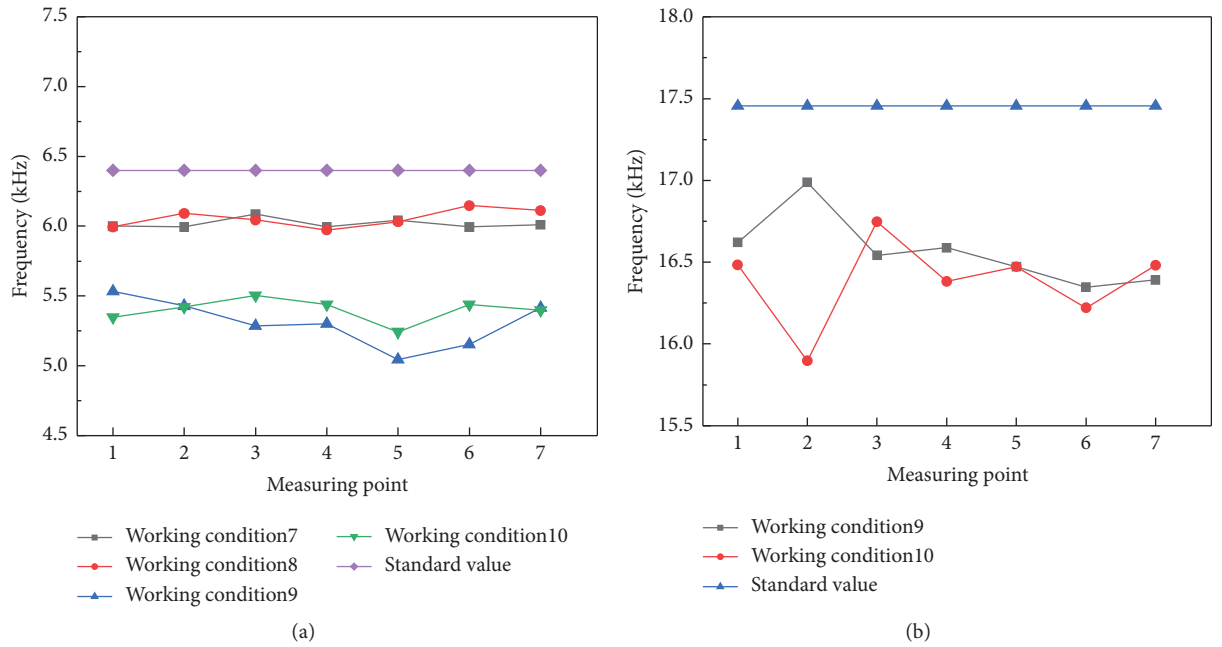

Figure 7: Frequency diagram of measuring points on the 3# board. (a) Board thickness frequency chart. (b) Defect frequency chart.

10, and most of the errors are between 4.2% and 7.1%. In addition, the reflection frequency rate of the steel bundle is concentrated between 8972 kHz and 9372 kHz at condition 7 and detected. The error is between 1.8% and 10.6% compared with the theoretical value of 8814 kHz, which shows that the steel bundle does not affect the detection of grouting defects by the impact-echo method.

5. Conclusion

Through the mutual verification of finite element analysis and field test, the following conclusions can be drawn:

(1) The impact echo method can effectively measure the location and depth of defects, and the pipeline material has an impact on the test results. The effects of metal bellows are smaller than that of PVC pipes, and the accuracy is higher. In addition, the larger the frequency drift rate of plate thickness is, the larger the transverse size of the defect is. Therefore, the defect depth can be quantitatively judged by combining the frequency drift rate of plate thickness with the measured defect depth.

(2) The critical surface of the defect and the testing surface influence the test results. When they are perpendicular to each other, it is not easy to detect them. And the detection error of defect depth is significant.

(3) When the longitudinal reinforcement is small, the reflection signal of the longitudinal support can hardly be detected, so it does not influence the detection of the main test signals such as defects and prestressing tendons. It is difficult for the prestressing steel bar to detect the beam signal when there is a defect, but it does not affect the defect depth signal test.

Data Availability

The data are included within the article.

Conflicts of Interest

The authors declare that there are no conflicts of interest regarding the publication of this paper.

References

[1] R. Woodward, L. Blake, W. Sketch et al., "Discussion. Collapse of ynys-y-gwas bridge, west glamorgan," *Proceedings - Institution of Civil Engineers*, vol. 86, no. 6, pp. 1177–1191, 1989.

[2] B. Mathy, R. Demars, F. Roisin, and M. Wouters, "Wouters.Investigation and strengthening study of twenty damaged bridges: a Belgium case history," in *Proceedings of the 3rd International Conference on bridge Management*, pp. 658–666, Guildford, UK, 1996.

[3] G. F. Xing, Z. X. Wang, J. H. Liu et al., "Research on compactness testing technology of box girder prestressed pore slurry," *Highway Traffic Science and Technology*, vol. 27, no. S1, pp. 114–117+121, 2010.

[4] H. Liu, C. Chen, Z. Guo, Y. Xia, X. Yu, and S. Li, "Overall grouting compactness detection of bridge prestressed bellows based on RF feature selection and the GA-SVM model," *Construction and Building Materials*, vol. 301, Article ID 124323, 2021.

[5] H. Liu, Y. Qi, Z. Chen, H. Tong, C. Liu, and M. Zhuang, "Ultrasonic inspection of grouted splice sleeves in precast concrete structures using elastic reverse time migration method," *Mechanical Systems and Signal Processing*, vol. 148, Article ID 107152, 2021.

[6] T. Maruyama, "Harmonic balance-boundary element and continuation methods for steady-state wave scattering by interior and surface-breaking cracks with contact acoustic nonlinearity," *International Journal of Solids and Structures*, vol. 210-211, pp. 310–324, 2021.

[7] M. Janku, P. Cikrle, J. Grosek et al., "Comparison of infrared thermography, ground-penetrating radar and ultrasonic pulse echo for detecting delaminations in concrete bridges," *Construction and Building Materials*, vol. 225, no. 20, pp. 1098–1111, 2019.

[8] N. J. Carino and M. Sansalone, "Detection of voids in grouted ducts using the impact-echo method," *Materials Journal*, vol. 89, no. 3, pp. 296–303, 1992.

[9] M. Hill, J. McHugh, and J. D. Turner, "Cross-sectional modes in impact-echo testing of concrete structures," *Journal of Structural Engineering*, vol. 126, no. 2, pp. 228–234, 2000.

[10] P.-L. Liu, L.-C. Lin, Y.-Y. Hsu, C.-Y. Yeh, and P.-L. Yeh, "Recognition of rebars and cracks based on impact-echo phase analysis," *Construction and Building Materials*, vol. 142, no. Jul.1, pp. 1–6, 2017.

[11] J. M. Kang, S. Song, D. Park, and C. Choi, "Detection of cavities around concrete sewage pipelines using impact-echo method," *Tunnelling and Underground Space Technology*, vol. 65, pp. 1–11, 2017.

[12] W. Jiang, Y. Xie, J. Wu, J. Guo, and G. Long, "Identifying bonding interface flaws in CRTS III type ballastless track structure using the impact-echo method," *Engineering Structures*, vol. 227, Article ID 111429, 2021.

[13] L. Yin, B. Ye, Z. Zhang et al., "A novel feature extraction method of eddy current testing for defect detection based on machine learning," *NDT & E International*, vol. 107, no. Oct., Article ID 102108, 2019.

[14] O. Abraham and P. Cote, "Impact-echo thickness frequency profiles for detection of voids in tendon ducts," *ACI Structural Journal*, vol. 99, no. 3, pp. 239–248, 2002.

[15] C. Colla, "Improving the accuracy of impact-echo in testing post-tensioning ducts," *AIP Conference Proceedings*, vol. 657, no. 1, pp. 1185–1192, 2003.

[16] R. Muldoon, A. Chalker, M. C. Forde, M. Ohtsu, and F. Kunisue, "Identifying voids in plastic ducts in post-tensioning prestressed concrete members by resonant frequency of impact-echo, SIBIE and tomography," *Construction and Building Materials*, vol. 21, no. 3, pp. 527–537, 2007.

[17] S. Dorafshan and H. Azari, "Evaluation of bridge decks with overlays using impact echo, a deep learning approach," *Automation in Construction*, vol. 113, Article ID 103133, 2020.